nature materials

ARTICLES

PUBLISHED ONLINE: 1 FEBRUARY 2016 | DOI: 10.1038/NMAT4561

Approaching theoretical strength in glassy carbon nanolattices

J. Bauer*, A. Schroer, R. Schwaiger and O. Kraft

The strength of lightweight mechanical metamaterials, which aim to exploit material-strengthening size effects by their microscale lattice structure, has been limited by the resolution of three-dimensional lithography technologies and their restriction to mainly polymer resins. Here, we demonstrate that pyrolysis of polymeric microlattices can overcome these limitations and create ultra-strong glassy carbon nanolattices with single struts shorter than 1 μm and diameters as small as 200 nm. They represent the smallest lattice structures yet produced—achieved by an 80% shrinkage of the polymer during pyrolysis—and exhibit material strengths of up to 3 GPa, corresponding approximately to the theoretical strength of glassy carbon. The strength-to-density ratios of the nanolattices are six times higher than those of reported microlattices. With a honeycomb topology, effective strengths of 1.2 GPa at 0.6 g cm^{-3} are achieved. Diamond is the only bulk material with a notably higher strength-to-density ratio.

Metamaterials are periodically patterned structures whose effective properties depend primarily on their topology rather than their composition[1]. They facilitate unique electrical, optical, or acoustic characteristics[1,2], but also combinations of mechanical properties that are in principle antagonistic, such as high stiffness and high damping capability[3], or negative Poisson's ratio[4]. Such property combinations can hardly be achieved by classical material design, which focuses on optimizing the chemistry and the microstructure of monolithic materials[5].

Micro- and nanostructuring additive manufacturing technologies[6–8] made an entirely new spectrum of characteristics such as optical cloaking[9] or broadband polarization[10] accessible[1,2]. Inspired by nature's hierarchical cellular materials[11], a miniaturization of lattice structures was achieved[12–14], yielding a class of lightweight mechanical metamaterials[15–17] whose effective properties are not determined only by their topology, but also by the microscopic length scale of their patterns. Lattice structures with stretching-dominated behaviour[5], such as fully triangulated frameworks, exhibit remarkable mechanical properties[18,19] at relative densities, $\bar{\rho}$, below 1% compared to the density of the bulk material, whereas the strength and stiffness of bending-dominated stochastic foams or non-rigid frame structures rapidly degrade when $\bar{\rho}$ decreases[5]. Microlattice materials combine a stretching-dominated topology with size-dependent strengthening related to the small-scale structural features.

Biological materials such as bone[20], enamel[21] or nacre[22] are composed of ceramic-like building blocks of the order of 1–100 nm in size, facilitating the exploitation of size-dependent material-strengthening effects[23]. The fracture strength of brittle materials is limited by the size of the flaws they contain. Therefore, the theoretical breaking strength of atomic bonds, which is considered of the order of $E/10$, with Young's modulus, E (ref. 24), generally cannot be reached. Because the size of flaws is limited by the overall dimensions of an object, it can be argued that the smaller the object, the higher its strength. On the nanometre scale, it has been discussed that the fracture strength, σ_f, of an object increases as $\sigma_f \propto 1/\sqrt{l_i}$ (ref. 23), with its dimensions, l_i, decreasing. Various examples of ultra-strong nanoscale objects such as 100 nm thin and 12 GPa strong silicon wires or carbon nanotubes (CNTs) and graphene reaching stresses as high as 100–130 GPa have been reported[24].

Polymeric microlattices with strut lengths of the order of 5–10 μm and strut diameters down to 1 μm can be fabricated[14–16] by three-dimensional (3D) direct laser writing[8] (3D-DLW), which is a two-photon lithography process. In combination with coating techniques, such as atomic layer deposition[25] (ALD), polymer–ceramic composites[15] and hollow ceramic structures[14,16] achieving remarkable strengths at densities well below 1 g cm^{-3} have been presented.

Nevertheless, two factors limit the attainable strength of microlattices. First, the resolution of available 3D manufacturing technologies does not allow the fabrication of lattices with smaller strut dimensions. Resolutions below 100 nm, which are typical of 2D processes such as electron-beam lithography, are desirable, but cannot be reached[26]. Second, lithographic processes require the use of polymeric resists with much lower stiffness and strength compared to ceramic materials. If smaller structural features could be made directly from a stronger and stiffer material, strength limitations[13,15,27] and buckling problems[14–16] could be overcome. Overall, the specific strength—that is, the ratio of strength to density—of the microlattices fabricated so far is only slightly improved compared to macroscopic lattices made from high-strength bulk materials[19].

By pyrolysis, structures from ultraviolet-cured polymer resins can be transformed into considerably smaller carbon structures with significantly enhanced physical properties. Carbon micro-electromechanical systems[28–30], as well as metamaterials serving as electrodes[31] or for energy absorption[32], have been presented. During pyrolysis, resins are thermally decomposed in vacuum or inert atmosphere at temperatures in the range of 1,000–3,000 °C (ref. 28). Accompanied by shrinkage of up to 90% (ref. 30), glassy carbon structures are formed. Glassy carbon is a disordered carbon allotrope primarily consisting of non-graphitic sp^2-bonded carbon[30,33]. It exhibits excellent chemical resistance, thermal stability and biocompatibility, and can achieve semiconductor-type electrical properties[30]. Its low density of 1.3–1.5 g cm^{-3} (refs 28,33) is attributed to a fullerene-related closed-celled porosity[34]. Its Young's modulus of 20–30 GPa (refs 33,35) is about ten times higher than that of crosslinked epoxy resins such as SU-8 (ref. 36).

Institute for Applied Materials, Karlsruhe Institute of Technology, 76131 Karlsruhe, Germany. *e-mail: jens.bauer@kit.edu

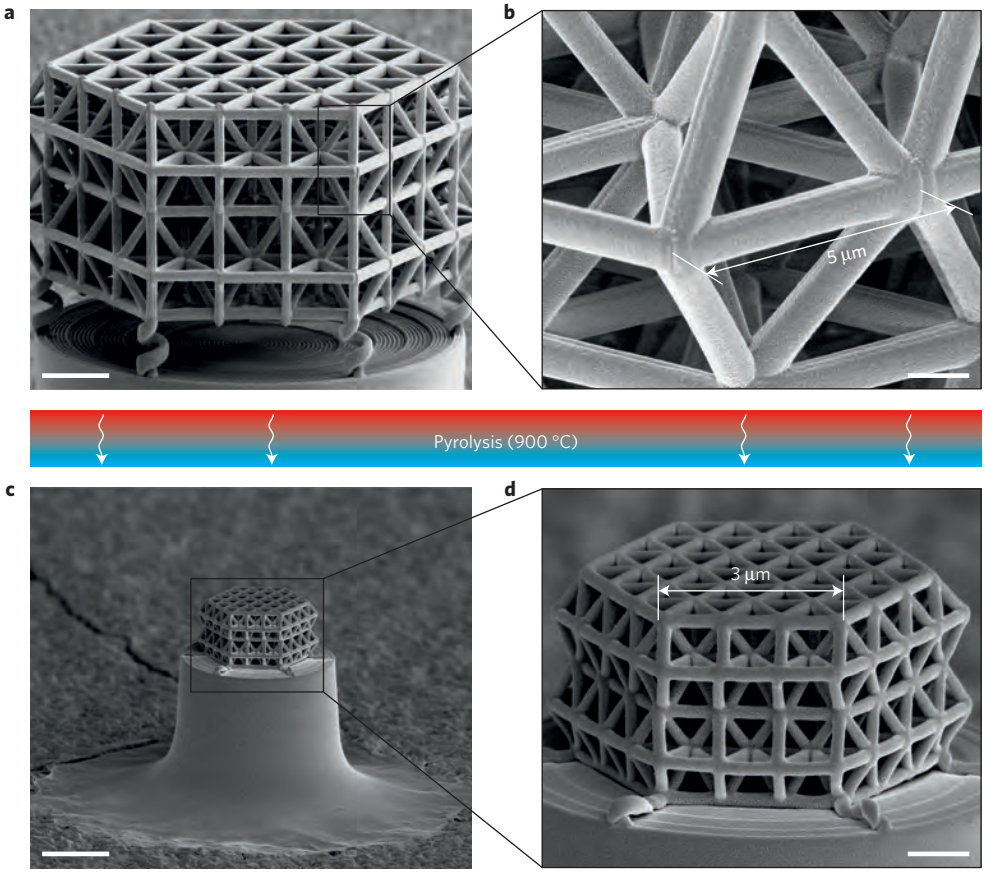

Figure 1 | Pyrolysis of 3D-printed polymeric microlattices creates glassy carbon nanolattices. a,**b**, Polymer structure before pyrolysis: whole structure (**a**) and close-up view of a single unit cell (**b**). **c**,**d**, Facilitated by a supporting construction, which decouples the structures from the substrate, the nanolattices isotropically shrink to about 20% of their initial size during pyrolysis. The magnifications of **a** and **c** (scale bars 5 μm), and also **b** and **d** (scale bars 1 μm), are identical.

In this paper, we present ultra-strong, lightweight nanoarchitected glassy carbon lattices. By pyrolysis of polymeric structures, which were produced using 3D-DLW, carbon nanolattices with single struts shorter than 1 μm and strut diameters of 200 nm were fabricated (Fig. 1). This feature size is five times smaller than what can be achieved by 3D-DLW directly. Our nanolattices, thus, represent the smallest lattice structures produced so far. Regarding mechanical metamaterials, the advantages of this procedure are evident, as we will show. However, this miniaturization also has great potential for other metamaterials—especially optical metamaterials. Our nanolattices sustained compressive stresses of up to 310 MPa at a density of 0.35 g cm^{-3}. Their specific strength exceeds that of most bulk materials and is six times higher than that of microarchitected lattices[15,16]. Nano-honeycomb structures fabricated in the same way exhibit compressive strengths of up to 1.2 GPa at 0.6 g cm^{-3}, leaving diamond as the only bulk material reaching a notably higher ratio of strength to density. Material stresses at failure were calculated to reach values in the range of 2–3 GPa, which corresponds to the theoretical strength of bulk glassy carbon.

The fabrication of carbon nanolattices and nano-honeycombs starts with writing polymeric microstructures by 3D-DLW. We manufactured lattices with tetrahedral unit cells of three different sizes, with strut lengths of 10, 7.5 and 5 μm, as well as honeycombs with triangular unit cells with an edge length of 5 μm. The structures were subsequently pyrolysed in vacuum at 900 °C. During pyrolysis, they shrank drastically to 20% of their original size. Nearly isotropic shrinkage (Fig. 1) was achieved by placing the structures on pedestals and coiled springs for decoupling from the substrate. Less rigid structures supported by topologically more restricted designs often experience large 'chewing gum-like' distortions[31] in one or several directions. Here, we created nearly undistorted lattice and honeycomb structures with unit cell edge lengths of only 2,020 nm, 1,440 nm and 970 nm (Fig. 2a–c). The walls of the honeycombs are only 140 nm in thickness. Cross-sections of the lattice struts are almost circular, with mean diameters decreasing from 305 to 215 nm from the largest to the smallest size. These values exceed the theoretical lateral resolution[26] of the elliptically shaped single line features of 3D-DLW by more than a factor two. However, the theoretical resolution is generally not reached in practice[26]. Therefore, the feature sizes demonstrated here are about five times smaller than those of the smallest lattice structures produced by 3D-DLW or other fully 3D manufacturing processes[13–17]. Thus, the term nanoarchitecture here literally refers to structures with unit cell and feature dimensions smaller than 1 μm. By X-ray photoelectron spectroscopy, the atomic bonds were found to be predominantly carbon-to-carbon for the pyrolysed structures, confirming the transformation from a crosslinked polymer to a pure carbon-based material. For mechanical characterization, we performed uniaxial *in situ* and *ex situ* compression tests using nanoindentation systems equipped with flat punch tips as described previously[15,27]. Two batches of samples—carbon-only structures and carbon structures with additional 10 nm-thin alumina coatings—were tested. For further fabrication and characterization details see the Methods section.

Figure 2d shows stress–strain curves for the three differently sized carbon lattices. From the largest to the smallest size, the compressive strength increases from 50 to 300 MPa and the stiffness from 1 to 3 GPa, while simultaneously the relative density changes from 13 to 25%. Correspondingly, strength and stiffness scale

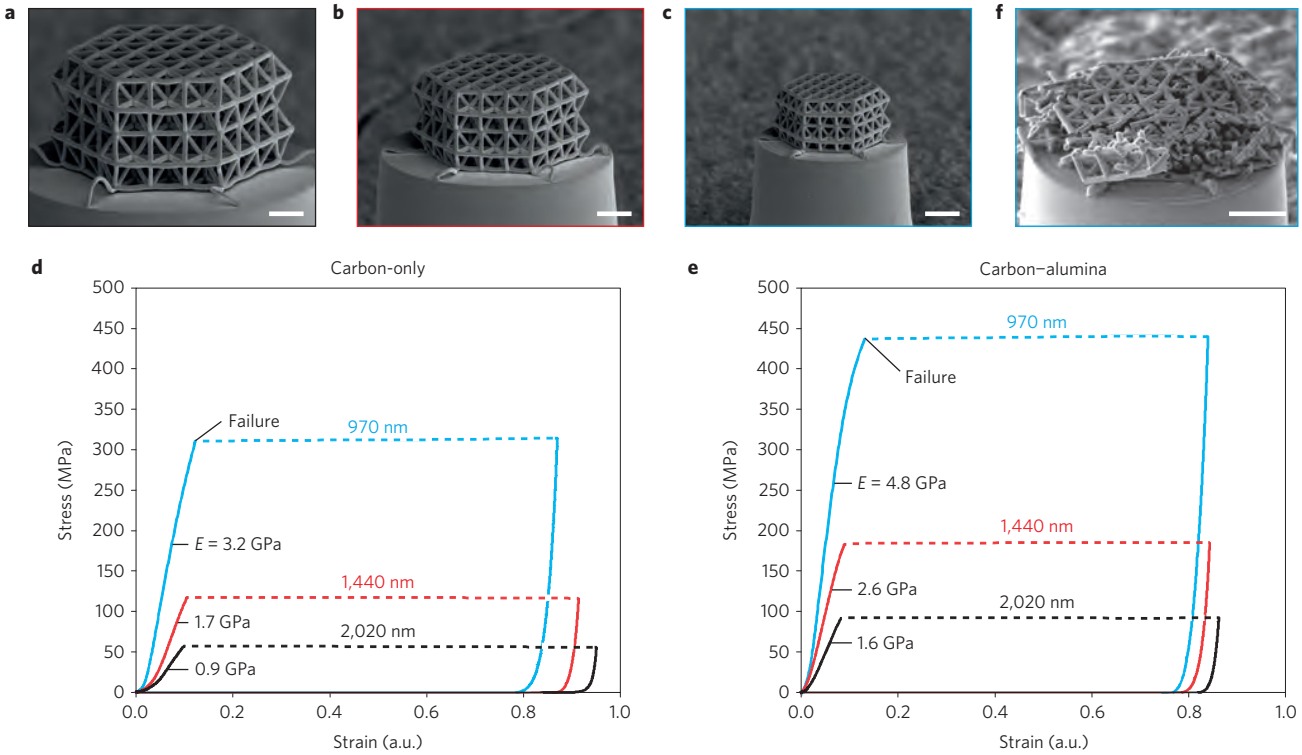

Figure 2 | Compression experiments of pyrolysed lattices with tetrahedral unit cells. a–c, SEM images of carbon lattices with strut lengths of 2,020 nm (**a**), 1,440 nm (**b**) and 970 nm (**c**). **d**, Stress–strain curves showing that strength and stiffness increase with decreasing dimensions (there are no data points recorded for the dashed parts of the curves). **e**, Stress–strain curves for lattice structures with the same dimensions, reinforced with 10 nm alumina coatings applied by ALD; strength and stiffness are enhanced further compared to the corresponding carbon-only structure shown in **d**. **f**, SEM micrograph of a fractured carbon-only structure (strut length: 970 nm), showing mostly brittle failure. All scale bars are 2 μm.

as the power of 2.3 and 1.67, respectively. For structures coated with 10 nm alumina layers, both the compressive strength and the stiffness of all lattices increase notably (Fig. 2e). For the smallest size, stresses and Young's moduli of up to 450 MPa and 5 GPa, respectively, are reached. However, the relative gain in strength compared to carbon-only structures decreases when the lattice size becomes smaller. Except for the nonlinear behaviour at small strains, which is related to misalignment, roughness and imperfections, linear-elastic behaviour followed by brittle failure is found for all structures, with and without alumina coatings. Figure 2f shows a carbon lattice (strut length 970 nm) which failed by brittle crushing (Supplementary Movie 1).

Pyrolysed honeycomb structures reached compressive strengths and Young's moduli of up to 1.2 GPa and 10 GPa, respectively. Figure 3a shows the corresponding stress–strain curve; the nominal stress–strain behaviour of the material has been determined analytically from the stress–strain behaviour of the honeycomb structure by considering its relative density of 43.7%. From this estimate, we determined Young's modulus of the material as 22.5 GPa, which agrees well with literature values of 20–30 GPa for glassy carbon[33,35]. At failure, nominal material stresses of 2.3–2.8 GPa were reached in the honeycombs, which is in the range of $E/10$ of bulk glassy carbon. These values should be considered as the lower bound, because we did not account for possible structural imperfections. Higher values were determined by finite element simulations, which are described in the Supplementary Information. As for the lattices, linear-elastic behaviour followed by brittle failure is observed for the honeycombs. Figure 3b shows a structure before testing. When unloading before the compressive strength is reached, flattening of the top surface and small cracks can be seen (Fig. 3c). Structures eventually crush in a brittle manner (Fig. 3d), with the fracture surfaces being partially sharply jagged (Fig. 3e).

For comparison, the nominal uniaxial stresses at failure in single lattice struts were estimated analytically, assuming an ideally pin-jointed assembly. We determined values of 1.6–2.1 GPa for the smallest lattice size. This is comparable to obtained nominal stresses in the walls of the honeycomb structures. With increasing strut size, however, the attained stresses in the struts decrease to 1.2 GPa and 0.75 GPa. Considering superimposed bending, which is typical of frozen truss joints, as well as geometrical edge effects and imperfections, again higher Young's moduli and stress maxima in the range of 1.4–3.5 GPa from the largest to the smallest lattice were determined by finite element simulations. See the Supplementary Information for analytical and numerical studies.

Figure 4 shows a compressive strength–density Ashby chart. The carbon and carbon–alumina lattices and honeycombs of this work are compared to other microarchitected and macroscopically structured lattice materials[15,16,19,37], to carbon-nanotube-based aerogels[38], as well as to commercial bulk materials. The strength of architected cellular materials ideally scales in a linear fashion for stretch-dominated behaviour with the relative and the absolute densities[5], which in the double-logarithmic plot corresponds to a line with a slope of 1 (dashed guidelines). Correspondingly, the theoretically achievable limit is indicated, with the lower bound defined by diamond, which has the highest specific strength of all bulk materials, and with the upper bound given by the strength of CNTs and graphene, representing the highest strength values measured so far. We determined the density of all our lattice and honeycomb structures by scanning electron microscopy (SEM)-measured dimensions as well as the density of glassy carbon and ALD alumina, for which a value of 3.0 g cm^{-3} was used. Our carbon lattices achieve strength-to-density ratios which markedly exceed those of all natural and technical cellular solids as well as those of macro- and microarchitected lattice materials. In particular,

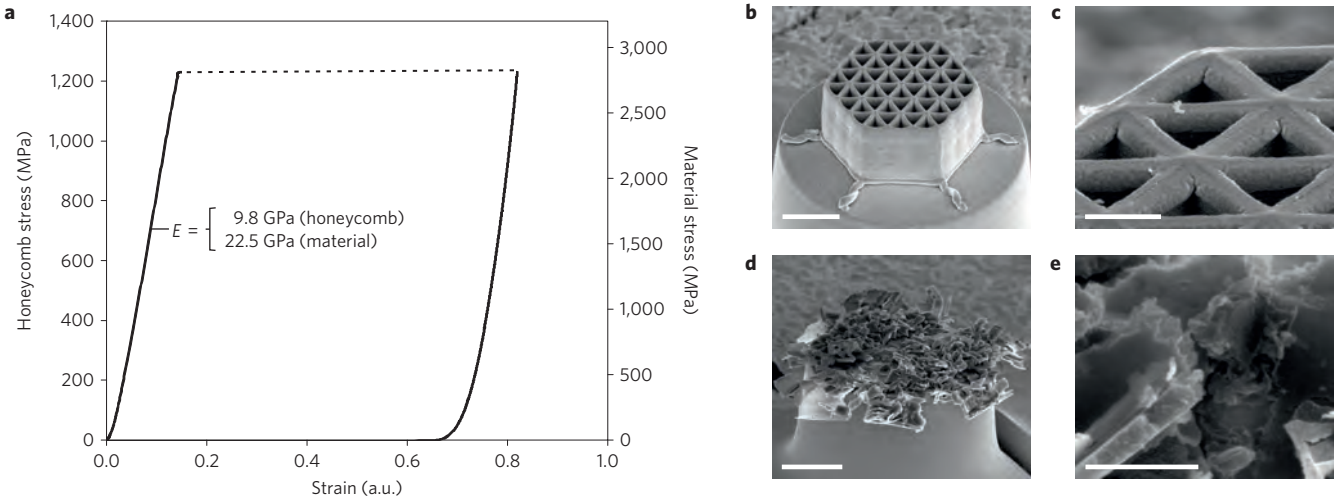

Figure 3 | Compression experiment of a pyrolysed honeycomb structure. a, Measured stress–strain curve for a carbon honeycomb with triangular unit cells with an edge length of 970 nm. The corresponding material stresses are shown on the right *y*-axis (there are no data points recorded for the dashed part of the curve). **b**, SEM image before testing. **c**, Close-up view of the structure loaded to 90% of the average compressive strength. **d**, Crushed structure after testing. **e**, Close-up view of a shell fragment from **d**. Scale bars are 2 μm (**b**,**d**) and 500 nm (**c**,**e**).

they have significantly higher strengths than glassy carbon lattices with millimetre-size unit cells as well as randomly structured carbon-nanotube-based aerogels. The highest specific strengths of alumina–polymer composites and hollow alumina microlattices, which have been the benchmark in the field of lightweight metamaterials, are outperformed by a factor of six. With densities in the range of only 0.16–0.38 g cm^{-3}, they are superior to most bulk materials. The observed increase of the strength when additional alumina coatings are applied (Fig. 2) involves an increase of the density as well. However, the gain in strength is higher, leading to an additional enhancement of the specific strength, which increases from less than 10% for the smallest lattice to more than 20% for the largest lattice. With a compressive strength of 1.2 GPa at 0.6 g cm^{-3} nanoarchitected carbon honeycombs achieve specific strengths close to the lower bound of the theoretical limit, exceeding any bulk metallic, polymeric and composite material, as well as most technical ceramics. For uniaxially loaded honeycombs, whose entire material ideally is aligned with the applied loading direction, the same specific strength can be achieved as for the respective monolithic material. In contrast, for tetrahedral lattice structures, the specific strength is by a factor of at least 1.5 (ref. 39) lower despite a linear scaling behaviour with the density. Accordingly, the theoretical limit for such a lattice is lower by the same factor with respect to the limit marked in Fig. 4. Therefore, similar to the honeycombs, the smallest lattices presented here achieve values close to the lower bound of that limit. The numerical values of all experimental results are given in Supplementary Table 1.

We demonstrated that pyrolysis of polymeric microarchitectures, which are patterned by 3D-DLW, yields carbon lattice materials with a significantly reduced feature size and unprecedented specific strength. This is achieved by a triangulated stretching-dominated cellular topology with nanoscale features. At this small scale, in the range of 200 nm, pronounced mechanical size effects come into play and the strut material may reach the theoretical strength of bulk glassy carbon. Neither macroscopic glassy carbon lattices nor randomly structured carbon-nanotube-based aerogels can reach the specific strength of the carbon nanolattices presented here. This demonstrates both the importance of taking advantage of size effects and an ordered architecture, pointing to the ideal material consisting of highly ordered nanotube-based lattices.

Although adding alumina coatings to the carbon lattice materials further enhances the strength, the gain in specific strength is fairly small. This is in contrast to polymeric structures where a significant increase was achieved by coatings[15]. This relates to the fact that both the strength of the 10 nm alumina coatings with 5.5 GPa (ref. 27) and the density are about twice as high as the respective values for the glassy carbon observed here. Thus, the specific strengths are comparable. Although direct-laser-written polymer templates are still needed, we conclude that pyrolysis can be considered an alternative to other post-process routes[12–17]. Up to this point, several steps were needed to create ceramic or metallic microlattices, including impression or coating techniques as well as focused ion beam milling and plasma etching for removal of the polymeric resist.

The scaling behaviour[40] of stiffness and strength of cellular materials with the relative or absolute density correlates with the present mechanical behaviour and the governing failure mechanism, both ideally scale linearly[5]. Despite the stretching-dominated topology here, a scaling exponent of 1.67 was obtained for the stiffness of the carbon lattices. This may be related to superimposed bending, as the lattice joints are frozen as well as the finite size of our structures, which introduces additional compliance at the outer elements. Comparable exponents have been found with alumina microlattices[16]. The strength of our carbon lattices scales according to an approximate power of two (Fig. 4), pointing towards buckling as the controlling failure mechanism[40]. This has been confirmed by correlating the experimental data to established analytical models[39,41] as well as to finite element simulations (Supplementary Figs 2 and 4). For the smallest lattice, nominal and peak material stresses at failure of 2–3 GPa were determined. This is in the range of the theoretical strength of bulk glassy carbon, indicating that material failure may become the strength-limiting factor. Also, it can be argued that buckling may not be relevant for the smallest lattice, as an additional stiffness-increasing alumina coating has only a minor effect on the specific strength, whereas notable increases are found for the two larger lattices. Because the strength-to-density ratios of both materials are comparable but the alumina is much stiffer[42] than glassy carbon, additional gains relate to an enhanced buckling strength, which depends on Young's modulus and not on the strength of the material. Buckling of lattices comprised of struts with length-to-diameter-ratios of only 5–8 is somewhat unexpected. However, as mechanical size effects strongly influence the attainable material strength, buckling which is not size-dependent becomes much more critical. This further illustrates the crucial role of extreme miniaturization, which is

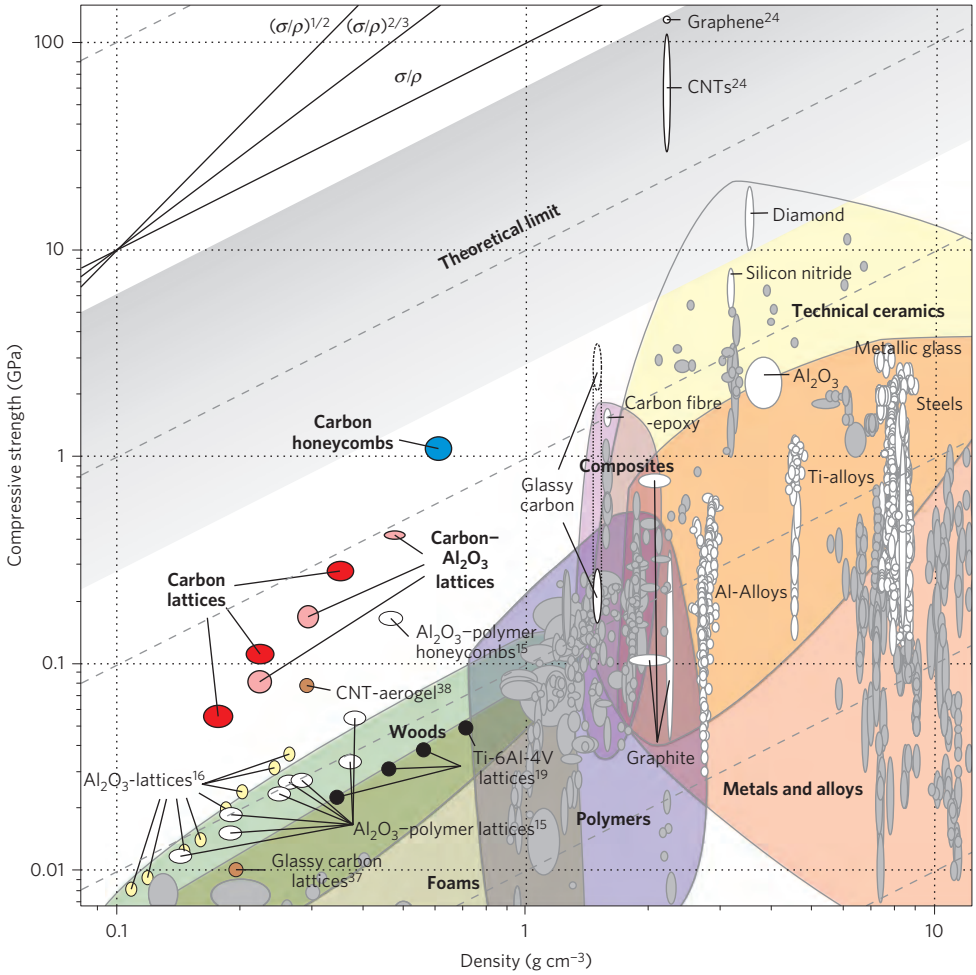

Figure 4 | Compressive strength–density Ashby map. This chart compares the carbon and carbon–alumina lattices and honeycombs of this study against other architected materials reported so far, natural and technical cellular solids, and monolithic bulk materials. Material properties are obtained from the Software CES Edupack 2014 (Granta Design), apart from those with an individual reference number.

needed for a lattice to exploit material strengths in the range of the theoretical limit.

To further elucidate this argument, we correlate the fracture strength, σ_f, of a brittle material with the critical size of a flaw, a_c, as given by $\sigma_f = YK_{IC}/\sqrt{\pi a_c}$, with the fracture toughness, K_{IC}. For an almond-shaped surface crack along the diameter of a cylinder loaded in tension or bending, which may be considered a typical crack geometry and load situation for a lattice with solid near-circular struts, the non-dimensional parameter, Y, is close to unity[43] if the crack depth is less than 30–40% of the diameter. The bulk strength of glassy carbon is in the region of 200 MPa (ref. 44), which is not much higher than that of crosslinked epoxy resins[36]. With $\sigma_f = 200$ MPa, and $K_{IC} = 0.91$ MPa m$^{0.5}$ (ref. 35), a critical flaw size of 6.6 μm can be estimated from the above fracture criterion, showing that the strength must increase as dimensions become small. Strengths of up to 2 GPa were found for glassy carbon fibres of 5 μm diameter[45], corresponding to a flaw size of 66 nm. Because the struts of the lattices in this work are only 200–300 nm in diameter they are unlikely to contain flaws larger than that. Therefore, it is not unexpected that values in the range of the theoretical limit of bulk glassy carbon of 2–3 GPa are reached. As has been discussed in refs 23,27, this would imply that eventually structures become flaw-insensitive, because the presence of flaws smaller than 30–70 nm would no longer affect the attainable strength. One could argue that the only possibility to achieve a further increase in strength is to make the struts from a CNT-like material. This may be feasible because Young's modulus of pyrolytic carbon has been discussed as increasing in the range below a few tens of nanometres[46]. Such behaviour has been attributed to a scale-driven high impact of surface effects[46], which may cause intensified graphitization. Values of 60–70 GPa have been reported for glassy carbon on the micro- and the nanoscale[45,46], suggesting these materials could also exhibit higher strengths. Stresses above 3 GPa as computed in this study may support this concept.

Pyrolysis has been shown to be an excellent method to increase the resolution of 3D direct-laser-written structures. Pushing fully 3D patterning with precisely controllable feature dimensions further into the nanoscale promises benefits from many physical phenomena. This potentially has impact beyond the field of lightweight mechanical metamaterials. For instance, first experiments with stimulated-emission-depletion direct laser writing[26] (STED-DLW), which is a modified 3D-DLW method with a resolution above the Abbe diffraction limit, facilitating features smaller than 200 nm, showed optical cloaking at visible wavelengths. However, even STED-DLW is still a microtechnology rather than a nanotechnology, and cannot reach resolutions achieved by 2D electron-beam lithography[26]. Combining STED-DLW and pyrolysis may facilitate 3D structures with features as small as 10 nm. We would then enter a size regime in the range of reported diameters of multiwall CNTs (ref. 47) and potentially have the chance to take advantage of their high strength and stiffness in nanolattice materials.

Methods

Methods and any associated references are available in the online version of the paper.

Received 23 July 2015; accepted 5 January 2016; published online 1 February 2016

References

1. Christensen, J., Kadic, M., Wegener, M. & Kraft, O. Vibrant times for mechanical metamaterials. *MRS Commun.* **5,** 453–462 (2015).
2. Lee, J. H., Singer, J. P. & Thomas, E. L. Micro-/nanostructured mechanical metamaterials. *Adv. Mater.* **24,** 4782–4810 (2012).
3. Salari-Sharif, L., Schaedler, T. A. & Valdevit, L. Energy dissipation mechanisms in hollow metallic microlattices. *J. Mater. Res.* **29,** 1755–1770 (2014).
4. Bückmann, T. *et al.* Tailored 3D mechanical metamaterials made by dip-in direct-laser-writing optical lithography. *Adv. Mater.* **24,** 2710–2714 (2012).
5. Fleck, N. A., Deshpande, V. S. & Ashby, M. F. Micro-architectured materials: past, present and future. *Proc. R. Soc. Lond. A* **466,** 2495–2516 (2010).
6. Jacobsen, A. J., Barvosa-Carter, W. & Nutt, S. Micro-scale Truss structures formed from self-propagating photopolymer waveguides. *Adv. Mater.* **19,** 3892–3896 (2007).
7. Zheng, X. *et al.* Design and optimization of a light-emitting diode projection micro-stereolithography three-dimensional manufacturing system. *Rev. Sci. Instrum.* **83,** 125001 (2012).
8. von Freymann, G. *et al.* Three-dimensional nanostructures for photonics. *Adv. Funct. Mater.* **20,** 1038–1052 (2010).
9. Arpin, K. A. *et al.* Multidimensional architectures for functional optical devices. *Adv. Mater.* **22,** 1084–1101 (2010).
10. Gansel, J. K. *et al.* Gold helix photonic metamaterial as broadband circular polarizer. *Science* **325,** 1513–1515 (2009).
11. Fratzl, P. & Weinkamer, R. Nature's hierarchical materials. *Prog. Mater. Sci.* **52,** 1263–1334 (2007).
12. Schaedler, T. A. *et al.* Ultralight metallic microlattices. *Science* **334,** 962–965 (2011).
13. Zheng, X. *et al.* Ultralight, ultrastiff mechanical metamaterials. *Science* **344,** 1373–1377 (2014).
14. Jang, D., Meza, L. R., Greer, F. & Greer, J. R. Fabrication and deformation of three-dimensional hollow ceramic nanostructures. *Nature Mater.* **12,** 893–898 (2013).
15. Bauer, J., Hengsbach, S., Tesari, I., Schwaiger, R. & Kraft, O. High-strength cellular ceramic composites with 3D microarchitecture. *Proc. Natl Acad. Sci. USA* **111,** 2453–2458 (2014).
16. Meza, L. R., Das, S. & Greer, J. R. Strong, lightweight, and recoverable three-dimensional ceramic nanolattices. *Science* **345,** 1322–1326 (2014).
17. Gu, X. W. & Greer, J. R. Ultra-strong architected Cu meso-lattices. *Extreme Mech. Lett.* **2,** 7–14 (2015).
18. George, T., Deshpande, V. S. & Wadley, H. N. G. Mechanical response of carbon fiber composite sandwich panels with pyramidal truss cores. *Composites A* **47,** 31–40 (2013).
19. Dong, L., Deshpande, V. & Wadley, H. Mechanical response of Ti–6Al–4V octet-truss lattice structures. *Int. J. Solids Struct.* **60,** 107–124 (2015).
20. Weiner, S. & Wagner, H. D. The material bone: structure-mechanical function relations. *Annu. Rev. Mater. Sci.* **28,** 271–298 (1998).
21. Yilmaz, E. D., Bechtle, S., Özcoban, H., Schreyer, A. & Schneider, G. A. Fracture behavior of hydroxyapatite nanofibers in dental enamel under micropillar compression. *Scr. Mater.* **68,** 404–407 (2013).
22. Meyers, M. A., Lin, A. Y.-M., Chen, P.-Y. & Muyco, J. Mechanical strength of abalone nacre: role of the soft organic layer. *J. Mech. Behav. Biomed. Mater.* **1,** 76–85 (2008).
23. Gao, H., Ji, B., Jaeger, I. L., Arzt, E. & Fratzl, P. Materials become insensitive to flaws at nanoscale: lesson from nature. *Proc. Natl Acad. Sci. USA* **100,** 5597–5600 (2003).
24. Zhu, T., Li, J., Ogata, S. & Yip, S. Mechanics of ultra-strength materials. *MRS Bull.* **34,** 167–172 (2009).
25. George, S. M. Atomic layer deposition: an overview. *Chem. Rev.* **110,** 111–131 (2010).
26. Fischer, J. & Wegener, M. Three-dimensional direct laser writing inspired by stimulated-emission-depletion microscopy. *Opt. Mater. Express* **1,** 614–624 (2011).
27. Bauer, J. *et al.* Push-to-pull tensile testing of ultra-strong nanoscale ceramic-polymer composites made by additive manufacturing. *Extreme Mech. Lett.* **3,** 105–112 (2015).
28. Schueller, O. & Brittain, S. Fabrication and characterization of glassy carbon MEMS. *Chem. Mater.* **4756,** 1399–1406 (1997).
29. Wang, C., Jia, G., Taherabadi, L. H. & Madou, M. J. A novel method for the fabrication of high-aspect ratio C-MEMS structures. *J. Microelectromech. Syst.* **14,** 348–358 (2005).
30. Lim, Y., Heo, J., Madou, M. & Shin, H. Monolithic carbon structures including suspended single nanowires and nanomeshes as a sensor platform. *Nanoscale Res. Lett.* **8,** 492 (2013).
31. Burckel, D. B. *et al.* Lithographically defined porous carbon electrodes. *Small* **5,** 2792–2796 (2009).
32. Lee, J. H., Wang, L. F., Boyce, M. C. & Thomas, E. L. Periodic bicontinuous composites for high specific energy absorption. *Nano Lett.* **12,** 4392–4396 (2012).
33. Cowlard, F. C. & Lewis, J. C. Vitreous carbon—a new form of carbon. *J. Mater. Sci.* **2,** 507–512 (1967).
34. Harris, P. J. F. Fullerene-related structure of commercial glassy carbons. *Phil. Mag.* **84,** 3159–3167 (2004).
35. Zhao, J. X., Bradt, R. C. & Walker, P. L. J. The fracture toughness of glassy carbons at elevated temperatures. *Carbon N. Y.* **23,** 15–18 (1985).
36. Mcaleavey, A., Coles, G., Edwards, R. L. & Sharpe, W. N. Mechanical properties of SU-8. *MRS Proc.* **546,** 213–218 (1998).
37. Jacobsen, A. J., Mahoney, S., Carter, W. B. & Nutt, S. Vitreous carbon micro-lattice structures. *Carbon N. Y.* **49,** 1025–1032 (2011).
38. Shin, S. J., Kucheyev, S. O., Worsley, M. A. & Hamza, A. V. Mechanical deformation of carbon-nanotube-based aerogels. *Carbon N. Y.* **50,** 5340–5342 (2012).
39. Deshpande, V. S. & Fleck, N. A. Collapse of truss core sandwich beams in 3-point bending. *Int. J. Solids Struct.* **38,** 6275–6305 (2001).
40. Gibson, L. J. & Ashby, M. F. *Cellular Solids: Structure and Properties* 2nd edn, Vol. 2 (Cambridge Univ. Press, 1999).
41. Wadley, H. N. G. Multifunctional periodic cellular metals. *Phil. Trans. R. Soc. Lond. A* **364,** 31–68 (2005).
42. Berdova, M. *et al.* Mechanical assessment of suspended ALD thin films by bulge and shaft-loading techniques. *Acta Mater.* **66,** 370–377 (2014).
43. Liu, A. *ASM Handbook Volume 19, Fatigue And Fracture* 980–1000 (ASM International, 1996).
44. Bullock, R. E. & Kaae, J. L. Size effect on the strength of glassy carbon. *J. Mater. Sci.* **14,** 920–930 (1979).
45. Kawamura, K. & Jenkins, G. A new glassy carbon fibre. *J. Mater. Sci.* **5,** 262–267 (1970).
46. Manoharan, M. P., Lee, H., Rajagopalan, R., Foley, H. C. & Haque, M. A. Elastic properties of 4–6 nm-thick glassy carbon thin films. *Nanoscale Res. Lett.* **5,** 14–19 (2010).
47. Yakobson, B. I. & Avouris, P. in *Carbon Nanotubes: Synthesis, Structure, Properties, and Applications* (eds Dresselhaus, M. S., Dresselhaus, G. & Avouris, P.) 287–327 (Springer, 2001).

Acknowledgements

The authors thank M. Madou for stimulating discussions introducing us to the concept of pyrolysis of resist structures. Financial support of this work by the Robert Bosch-Foundation is gratefully acknowledged.

Author contributions

J.B. and O.K. designed the research; J.B. designed structures; J.B. and A.S. manufactured samples; J.B., performed *ex situ* measurements; J.B. and R.S. performed *in situ* measurements; J.B. performed analytical and finite element calculations; J.B., O.K. and R.S. analysed data; J.B. wrote the paper.

Additional information

Supplementary information is available in the online version of the paper. Reprints and permissions information is available online at www.nature.com/reprints. Correspondence and requests for materials should be addressed to J.B.

Competing financial interests

The authors declare no competing financial interests.

Methods

Fabrication. Manufacturing carbon lattices and honeycombs comprises two production steps. We first fabricated polymeric microarchitectures by 3D-DLW (Photonic Professional, Nanoscribe GmbH), in the dip-in laser lithography configuration[4] applying the photoresist IP-Dip (Nanoscribe GmbH). We manufactured three differently sized lattices with tetrahedral unit cells with edge or strut lengths, a, of 10, 7.5 and 5 μm (Supplementary Figs 1 and 3). Honeycombs with triangular unit cells were fabricated with an edge length of 5 μm, corresponding to the implemented length of a single cell wall, and a height, h, of 15 μm.

In the subsequent pyrolysis step, polymeric microarchitectures were converted into carbon nanostructures in a vacuum tube furnace. On the basis of the recipe described in ref. 30 the pyrolysis consists of two pre-baking steps for degassing and the major part of the volume reduction, as well as a carbonization step. Initially samples were heated to 250 °C at a ramp rate of 5 °C min^{-1} and maintained at that temperature for 45 min. We introduced this additional pre-bake step compared to ref. 30 because polymeric microarchitectures are known from previous studies[27] to withstand 250 °C without damage. Subsequently, the samples were heated to 350 °C at a ramp rate of 3 °C min^{-1} and maintained at that temperature for 60 min. Then the temperature was increased to 900 °C at the same rate and held constant at that value for 60 min. Finally, samples were cooled down to room temperature. A pedestal and coil spring construction was designed, which decouples the structures from the substrate, to assure nearly isotropic shrinkage during the pyrolysis (Fig. 1 and Supplementary Fig. 1). Carbon–alumina structures were fabricated by applying 10 nm-thin conformal alumina coatings by ALD at 250 °C (Savannah 100, CambridgeNanotechALD).

Characterization. During the pyrolysis, the unit cell sizes of our structures shrank by roughly 80% compared to the initially fabricated sizes, yielding lattices with unit cell edge lengths, a, of 2,020 nm, 1,440 nm and 970 nm, respectively, and honeycombs with an edge length of 970 nm. The struts of the pyrolysed lattices have elliptical cross-sections with axial diameters, d_1, of 330, 270 and 225 nm and lateral diameters, d_2, of 275, 235 and 205 nm, respectively, for the three different lattice sizes. Pyrolysed honeycombs are 3 μm high and their walls are 140 nm in thickness. All dimensions were measured optically by scanning electron microscopy. The relative densities, $\bar{\rho}$, (Supplementary Table 1) of the pyrolysed structures were calculated using the unit cell topologies (Supplementary Fig. 1) and the measured dimensions.

We investigated the composition of the pyrolysed structures by X-ray photoelectron spectroscopy (K-Alpha XPS+, Thermo Fisher Scientific) using a microfocused monochromated Al Kα X-ray source with a spot size of 30 μm. On the basis of spectra in the C1s region an amount of up to 86 at.% of carbon-to-carbon bindings was determined, confirming a low level of oxygen and hydrogen in the pyrolysed carbon structures. However, an exact measurement is challenging, because our structures with diameters of 6–12 μm are much smaller than the applied smallest available spot size of 30 μm. Therefore, a certain portion of the detected signal may come from the surrounding substrate.

To determine the effective densities of the carbon structures, we applied the calculated respective relative volume densities of the structures and the material density of glassy carbon of 1.3–1.5 g cm^{-3} (refs 28,33). Originating from the polymer structures made from IP-Dip, whose density is in the range of 1.3 g cm^{-3} (ref. 15), this agrees well with the observed shrinkage of 80% and reported mass losses during pyrolysis[48,49] of roughly 80%. With the density of ALD alumina deposited at 250 °C, which is in the range of 3 g cm^{-3} (ref. 50), the density of the carbon–alumina lattices was calculated analogously.

For mechanical characterization, we performed uniaxial *ex situ* compression tests at a constant displacement rate of 100 nm s^{-1} (Nanoindenter G200 XP, Agilent/Keysight Technologies), as well as loading-rate-controlled *in situ* experiments (InSEM, Nanomechanics), by nanoindentation with flat punch diamond tips with diameters of 50 μm (*ex situ*) and 100 μm (*in situ*). Load–displacement curves were recorded. Applying the measured cross-sectional area of the top face of the structures, A, and the structure height, engineering stress and strain were determined. The compressive strength of the structures, σ_c, is defined as the maximum compressive stress before collapse. Their Young's modulus, E_{eff}, was determined as the maximum slope of the corresponding stress–strain curve. Nonlinear behaviour at low strains is related to small misalignments between the indenter tip and the specimen, local surface roughness in the contact area, as well as structural imperfections of the specimen. Analytical and finite element studies are described in the Supplementary Information, corresponding numerical values are given in Supplementary Table 2.

References

48. Singh, A., Jayaram, J., Madou, M. & Akbar, S. Pyrolysis of negative photoresists to fabricate carbon structures for microelectromechanical systems and electrochemical applications. *J. Electrochem. Soc.* **149,** 78–83 (2002).
49. Kim, H.-J., Joo, Y.-H., Lee, S.-M. & Kim, C. Characteristics of photoresist-derived carbon nanofibers for Li-ion full cell electrode. *Trans. Electr. Electron. Mater.* **15,** 265–269 (2014).
50. Groner, M. D., Fabreguette, F. H., Elam, J. W. & George, S. M. Low-temperature Al_2O_3 atomic layer deposition. *Chem. Mater.* **16,** 639–645 (2004).